Astron. Astrophys. 326, 1090–1102 (1997)

ASTRONOMY
AND
ASTROPHYSICS

EUV spectroscopy of cool stars

III. Interpretation of EUVE spectra in terms of quasi-static loops

G.H.J. van den Oord[1], **C.J. Schrijver**[2], **M. Camphens**[1], **R. Mewe**[3], **and J.S. Kaastra**[3]

[1] Sterrekundig Instituut Utrecht, Postbus 80 000, 3508 TA Utrecht, The Netherlands
[2] Stanford-Lockheed Institute for Space Research, Dept. H1-12, Bldg. 252, 3251 Hanover Street, Palo Alto, CA 94304, USA
[3] SRON Laboratory for Space Research, Sorbonnelaan 2, 3584 CA Utrecht, The Netherlands

Received 26 March 1997 / Accepted 26 May 1997

Abstract. We discuss the limitations of coronal spectroscopy to derive physical parameters of stellar magnetic loops. We distinguish between the intrinsic non-uniqueness of emitted spectra for models of quasi-static coronal loops, and the supplemental ambiguity introduced by both instrumental effects and spectral line formation. We demonstrate that the spectrum emitted by loops with constant cross-sections is the same for a large range of values of the conductive flux at the base when the apex temperature is fixed. Because it is impossible to estimate the conductive flux at the base from observations, it is also impossible to determine the volume heating rate and the loop length uniquely. For geometrically expanding (tapered) loops, the emitted spectrum depends on the expansion and on the conductive flux at the base, and there is a trade off between them without significant changes in the spectrum. We show that loop length and heating rate can only be derived if the density is known, but that even then a large intrinsic uncertainty remains for these loop parameters. We conclude that there is no unambiguous relationship between loop parameters and emitted spectra: modeling the spectra as the sum of spectra from discrete loops cannot result in a unique determination of coronal structure.

Based on spectra observed with the Extreme Ultra Violet Explorer ($EUVE$) we find that quasi-static loop models allow adequate modeling of stellar coronal spectra. We show that coronal loops on active cool stars must expand with height. The minimum required areal expansion between base and apex is not very large, lying between 2 and 5. For three stars (α Cen, Capella and ξ UMa) the observations suggest the presence of two distinct, dominant loop populations, while for χ^1 Ori a single population, characterized by a single apex temperature, suffices. The high electron densities ($10^{12}-10^{13}$ cm^{-3}) for coronal components on Capella and ξ UMa require abnormally large heating rates. It is likely that these high densities are related to a multitude of small volumes that are temporarily excited.

Send offprint requests to: G.H.J. van den Oord

Key words: stars: coronae – α Cen – Capella – χ^1 Ori– ξ UMa – X-rays: stars

1. Introduction

One of the aims of X-ray and EUV spectroscopic observations is to derive information about the physical conditions which prevail in stellar coronae. Spectra with moderate to high resolution can provide such information about coronal temperatures, chemical abundances and, sometimes, densities. It is common practice to describe the properties of a spectrum in terms of the differential emission measure (DEM) which is a weighting function describing the contribution by the plasma, at each temperature, to the observed spectrum.

Although a spectrum contains many spectral lines, formed at different temperatures, the information contents of a spectrum is limited. This is caused by the fact that individual spectral lines have a finite formation width in temperature. As a result one cannot determine the DEM with arbitrarily good temperature resolution. In general a temperature resolution of $\Delta \log T \approx 0.1$ can be achieved when individual lines are resolved in the spectrum as is the case for $EUVE$ spectra.

As was already noted by Craig & Brown (1976), the DEM has a number of undesirable properties. It is an intrinsic property of the DEM to be low at temperatures associated with locations where strong temperature gradients exist while these are, from a physical point of view, the most interesting. Also the DEM depends in an undesirable way on the parameters which describe a coronal plasma, like the pressure, the temperature, the conductive flux and the loop geometry as is discussed in Sect. 4.

On an observational level the differential emission measure of a source is not a unique quantity. Its functional form depends on the instrument used for the observation, the source properties, the photon statistics, the inversion algorithm and the spectral code used for the spectral analyses. Consistency requires, however, that, when identical spectral codes are used,

the DEMs resulting from different inversion algorithms are not significantly different.

Recently we have analyzed the coronal EUV spectra of seven cool stars, solar-like single stars and components of RS CVn-like binaries, as observed with the spectrometers of the Extreme Ultraviolet Explorer ($EUVE$): α Cen, Procyon, Capella, ξ Uma, σ Gem, χ^1 Ori, and AU Mic during a major flare. The derived differential emission measure distributions indicate that the bulk of the coronal plasma is at temperatures between 2 MK and about 10 MK and that the DEM is low at temperatures below 1 MK (see Mewe et al. 1995 and Schrijver et al. 1995, hereafter Paper I and Paper II, respectively). In this paper we address the questions whether the observed DEMs are compatible with models of quasi-static coronal loops and, even more important, what information about coronal conditions and geometry can be derived from the observations. Quasi-static coronal loop models have been extensively studied (see van den Oord & Zuccarello, 1997, and references given therein) and have been used before to analyze observations (see, e.g., Schrijver et al. 1989, Ciaravella et al., 1996, 1997, Maggio & Peres, 1996).

Suppose that one wants to decompose an observed spectrum into the contributions by loops with different characteristics. One can calculate a large number of loop models, determine their differential emission measure distributions, generate a library of spectra (taking the instrumental properties into account) and fit these to the observed spectrum. In this way one approximates the observed spectrum as a sum of spectra of individual loops. The properties of the loops which provide the best fit are then assumed to represent the properties of the observed corona. In this paper we demonstrate, however, that coronal loops with very different physical properties have identical differential emission measure distributions and therefore identical spectra: there is no unique relation between the physical characteristics of a loop and its spectrum (or its DEM). This has serious implications for coronal diagnostics.

On another level there is a uniqueness problem related to the fact that for a specific instrument, differing spectra, related to different model DEM distributions, can be almost identical once they have been convolved with the instrumental response.

Despite the above mentioned uniqueness problems, and the impossibility to determine accurately coronal (loop) parameters, we show in this paper that, based on the comparison of an observed DEM and a model DEM, it is possible to make some statements about the global properties of the coronal loop

the same inversion algorithm. The model differential emission measure of a coronal loop (discussed in Sect. 4, see Fig. 4) has a shape that is characterized by 1) a gradual slope up to temperatures close to the maximum temperature, 2) a high value in the temperature bin which contains the maximum temperature and 3) a vertical drop to zero in the next temperature bin. Inversion algorithms have not (yet) been optimized to recover a DEM which combines the properties of a gradual and a discontinuous behaviour. However, for a given inversion algorithm, there exists a relationship between the functional form of a theoretical input DEM and its recovered version. Whether this relationship is unique has to be verified using simulations. Because the differential emission measure distribution of a coronal loop has a pronounced maximum around the maximum temperature of a loop, the emitted spectrum is dominated by spectral lines formed at these temperatures. It is, however, the gradual tail below the maximum temperature which contains most information about the (thermodynamical) loop structure.

In Papers I and II, and in the present paper, we use the method of statistical regularization to solve Eq. (1). For a detailed description we refer to Paper I. Our method requires that the second derivative of $D(T)$ is as smooth as is allowed by the spectral data. In a mathematical sense this implies that the differential emission measure is subjected to smoothing over, effectively, three adjacent temperature bins. The width of the temperature bins is taken equal to $\Delta \log T = 0.1$ so that the smoothing is over a temperature range $\Delta \log T \approx 0.3$, the typical formation width of spectral lines (cf. a factor two in temperature). The smoothing matches the temperature resolution permitted by the physics of line formation while, on the other hand, high-frequency oscillations of $D(T)$, due to the presence of noise, are suppressed.

We use the Utrecht spectral code SPEX (Kaastra et al., 1996b, Mewe et al., 1996b) to create spectra as would be observed with the $EUVE$ and to analyze these spectra. Abundances are expressed relative to solar photospheric abundances (Anders & Grevesse, 1989). The ionization balance of Arnaud & Rothenflug (1985) is used. We do not use the recent update for Fe (Arnaud & Raymond, 1992), because in Papers I and II the differential emission measure analyses are based on Arnaud & Rothenflug and changes in the spectral model would induce changes in the derived $D(T)$.

The photon statistics depend roughly on the total emission measure of the source EM, the source distance d and the observing time $t_{\rm obs}$. All observations described in Papers I and II are characterized by the product $EM d_{\rm pc}^{-2} t_{\rm obs}$ being of the order of 10^{55} cm^{-3}s. In our simulations we therefore set the parameters so that $EM d_{\rm pc}^{-2} t_{\rm obs}$ is always 10^{55} cm^{-3}s. An interstellar column density of 10^{18} cm^{-2} was assumed for all simulations.

3. *EUVE* observations

The Extreme Ultraviolet Explorer ($EUVE$, e.g., Bowyer & Malina, 1991) observed EUV spectra in the wavelength range of 64 Å up to 808 Å (although interstellar extinction limits that range effectively to about 500 Å for the nearest cool stars), with a resolution of 0.25 up to 1.0 Å depending on wavelength. We analyzed spectra of seven cool stars, as discussed in papers I and II. These papers also discuss the spectral codes and inversion strategies; Schrijver et al. (1994) discuss potential effects of resonant scattering in a few of the strongest spectral lines. A collection of other spectra and their modeling can be found in Bowyer & Malina (1996), and references therein. Fig. 1 shows several DEMs, including that of the Sun. In this paper we study only α Cen, Capella, ξ UMa and χ^1 Ori, in detail because these gave the best spectra.

The four sources modeled in this paper have several common characteristics: all have a clear peak around 1.5 MK up to 3 MK, with a minimum around 10 MK to 15 MK. Below the maximum, the rate of decrease differs from star to star. Below 10^5 K the DEM is dominated by a formal fit of the He II lines; the assumption of negligible optical thickness is incorrect for these lines, and the DEM merely reproduces the line strengths.

An interesting feature which was found in all observed differential emission measure distributions, except for χ^1 Ori, is an upturn at high temperatures. This 'tail' is found at temperatures for which only a few spectral lines are present in $EUVE$ spectra together with a featureless continuum in the SW band. As is discussed in Papers I and II, there are various explanations for the presence of this DEM tail. For some sources it is related to a hot coronal component, while for other sources it indicates that the line-to-continuum ratio differs from what is expected from the spectral model. This can occur when the metal abundances are lower than the assumed solar photospheric abundances. In the case of α Cen and, especially, Procyon there are strong indications that for certain (strong) spectral lines resonant scattering and subsequent photon destruction plays a role (Schrijver et al., 1994, 1996).

4. Quasi-static loop models and their DEMs

In this section we discuss the thermodynamical structure of quasi-static coronal loops and the associated differential emission measure. Quasi-static coronal loops are characterized by a local balance between heating, conduction and radiative losses. The equation for energy conservation can be written as a system of coupled nonlinear differential equations (see, e.g., Rosner et al., 1978, Vesecky et al., 1979 (hereafter VAU), van den Oord & Zuccarello, 1997)

$$\frac{dT}{ds} = -\frac{F_{\rm c}}{\kappa_0 T^{5/2}} \ , \tag{2}$$

$$\frac{dF_{\rm c}}{ds} = E_{\rm heat} - \frac{p^2}{4k^2}\frac{\Psi(T)}{T^2} - F_{\rm c}\frac{d\ln A}{ds} \ . \tag{3}$$

In these expressions s is the coordinate along the magnetic field, $A(s)$ the cross-section of the loop at position s, p the pressure, $T(s)$ the temperature, $E_{\rm heat}$ the volume heating and k Boltzmann's constant. The classical conductive flux per unit cross-section is given by $F_{\rm c}(s) = -\kappa_0 T^{5/2} (dT/ds)$ with $\kappa_0 = 8.8\ 10^{-7}$ erg cm^{-1} s^{-1} K$^{-7/2}$ (Spitzer, 1962). The radiative losses are given by $E_{\rm rad}(s) = n^2\ \Psi(T)$ (erg cm^{-3}s^{-1})

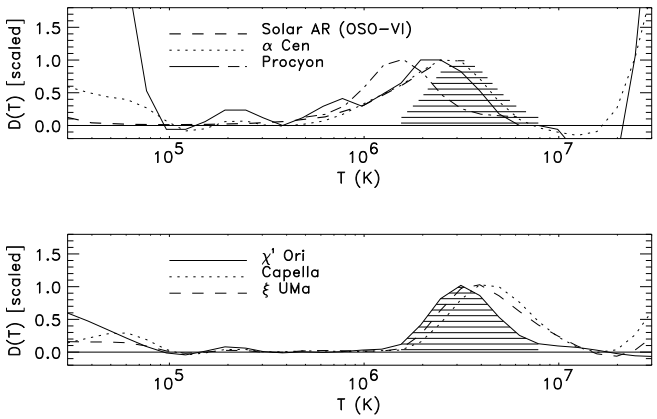

Fig. 1. Comparison of normalized emission measure distributions $D(T)$. The curves are normalized to unity around 3 MK. The distributions are smoothed over two temperature bins of $\log T = 0.1$. The dashed region in both panels is the DEM for χ^1 Ori between 1.5 MK and 8 MK. The data are taken from Papers I and II, although for Procyon we also show the DEM derived by Schmitt et al. (1996) (dashed – dotted line). The difference in the DEMs for Procyon – derived from the same $EUVE$ spectrum – demonstrates the sensitivity of the DEM to the inversion algorithm and the spectral code used.

with $\Psi(T)$ the emissivity. For the emissivity we used the piecewise power-law approximation given in van den Oord & Barstow (1988) although, for analytic purposes, the approximation $\Psi(T) = \Psi_0 T^{-1/2}$ with $\Psi_0 = 10^{-18.8}$ is occasionally used. The last term on the right-hand side of Eq. (3) accounts for the variation of the cross-section. Throughout this paper we assume that the pressure p and the heating $E_{\rm heat}$ are constant along a loop. These assumptions are discussed in Sect. 6. We assume that the loop plasma consists of fully ionized hydrogen, although in the emissivity both line and continuum radiation by other elements is taken into account.

The differential emission measure of a coronal loop can be written as

$$D(T) = \left(\frac{p}{2kT}\right)^2 \frac{Ads}{d\log T} = \left(\frac{\kappa_0 \ln 10}{4k^2}\right) \frac{p^2 A T^{3/2}}{|F_{\rm c}|} \ , \qquad (4)$$

where A and $F_{\rm c}$ are implicit functions of temperature T because $A = A(s(T))$ and $F_{\rm c} = F_{\rm c}(s(T))$. Eq. (4) immediately shows that the shape of the DEM is sensitive to the variations of the cross-section and the conductive flux. From now on we write $D(T)$ for $D(T)\Delta \log T$ so that $D(T)$ is the DEM integrated over a logarithmic temperature bin. The total emission measure within a certain temperature range then follows by summing the values of $D(T)$ for the relevant temperature bins.

4.1. Loops with constant cross-section

For loops with constant cross-section the last term in Eq. (3) is zero. At one temperature $T_{\rm i}$ in such a loop the heating balances locally the radiative losses, so $E_{\rm heat}/p^2 = \Psi(T_{\rm i})/(4k^2 T_{\rm i}^2)$. This relation represents one of the scaling laws (see, e.g., Rosner et al., 1978). Temperature $T_{\rm i}$ corresponds to the critical point of the system at which $dF_{\rm c}/ds = dT/ds = 0$. At this temperature the conductive flux has an extremum ($dF_{\rm c}/ds|_{T_{\rm i}} = 0$). From the base of the coronal loop upward, the conductive flux becomes increasingly negative and reaches its maximal negative value at $T = T_{\rm i}$. At locations above $s(T_{\rm i})$ the conductive flux goes to zero because at the apex of the loop the temperature reaches its maximum ($dT/ds = 0$, see the phase plane diagram in van den Oord & Zuccarello, 1996).

A first integral of the system of differential equations can be obtained by dividing the equations and integrating the resulting expression for $dF_{\rm c}/dT$. To simplify the analysis we use the approximate radiative loss curve $\Psi(T) \equiv \Psi_0/\sqrt{T}$ to obtain an analytic expression for the first integral. The temperature of the critical point is then given by $T_{\rm i}^{5/2} = \Psi_0 p^2/(4k^2 E_{\rm heat})$ and the first integral reads

$$\begin{aligned} F_{\rm c}^2(T) &= p^2\kappa_0 \left(f(T) - f(T_{\rm b})\right) + F_{\rm c}^2(T_{\rm b}) \\ &= p^2\kappa_0 \left(f(T) - f(T_{\rm a})\right) \end{aligned} \qquad (5)$$

with

$$f(T) = \frac{\Psi_0 T}{2k^2} - \frac{4}{7}\frac{E_{\rm heat}}{p^2} T^{7/2} = \frac{\Psi_0}{2k^2}\left(T - \frac{2}{7}\frac{T^{7/2}}{T_{\rm i}^{5/2}}\right) \ . \qquad (6)$$

In these expressions $T_{\rm b}$ and $T_{\rm a}$ are the temperatures at the base and at the apex, respectively. Note that $F_{\rm c}(T_{\rm a}) = 0$ is used in the second identity of Eq. (5). For given values of $T_{\rm b}$ and $T_{\rm a}$, Eq. (5) relates $E_{\rm heat}$, p and $F_{\rm c,b} \equiv F_{\rm c}(T_{\rm b})$. Using the first integral we can calculate the differential emission measure distribution and the loop length. The differential emission measure varies according to

$$D(T) \sim \frac{ApT^{3/2}}{\sqrt{f(T) - f(T_{\rm a})}} \ . \qquad (7)$$

The half-length of a loop follows from Eq. (2) and is given by

$$L = \frac{\sqrt{\kappa_0}}{p} \int_{T_{\rm b}}^{T_{\rm a}} \frac{T^{5/2}}{\sqrt{f(T) - f(T_{\rm a})}} dT \ . \qquad (8)$$

This expression is the second scaling law for coronal loops. The scaling law derived by Rosner et al. (1978) is based on the choice $T_{\rm b} = 0$ and $F_{\rm c,b} = 0$ which permits an analytical evaluation of the integral.

The stellar DEMs provide us with a good indication of the apex temperature: because $F_{\rm c}(T_{\rm a}) = 0$, $D(T_{\rm a}) \rightarrow \infty$ and the binned DEM, that is, $D(T)$ integrated over the temperature bins, has a maximum at $T_{\rm a}$. The base temperature $T_{\rm b}$ is taken equal to $3\ 10^4$ K. This temperature is sufficiently low to connect the coronal loop to the chromosphere and sufficiently high to guarantee that 1) radiative transfer effects are negligible (except for the He II lines, which fall below the temperature range that we consider in Sect. 5) and 2) the presence of neutrals does not affect the thermal conduction.

The above expressions for $D(T)$ and L have some interesting properties. First of all, the pressure acts as a multiplicative constant. Secondly, the only parameter in the integrand is temperature $T_{\rm i}$ (second identity in Eq. (6)). The slope of $D(T)$ and

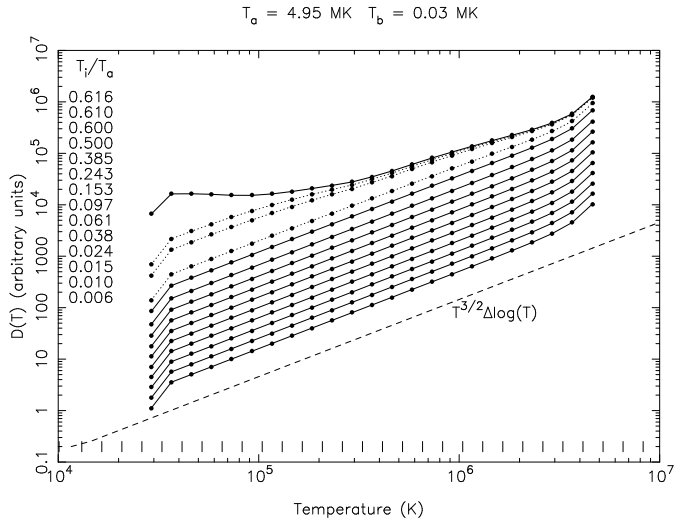

Fig. 2. Model DEMs for the allowed range of values of T_i at a fixed apex temperature T_a = 4.95 MK. The upper curve is for zero conductive flux at the base and, therefore, maximum value of T_i. Between each of the solid curves the ratio $T_\mathrm{i}/T_\mathrm{a}$ is lowered by a factor $10^{0.2}$ = 1.58. The dotted curves are for $T_\mathrm{i}/T_\mathrm{a}$ = 0.6, 0.55 and 0.5 from top to bottom. The dashed curve is given for comparison and indicates a $T^{3/2}$ distribution integrated over each (logarithmic) temperature bin. Note that for $T_\mathrm{i}/T_\mathrm{a} < 0.55$ the shape of $D(T)$ becomes completely independent of the actual loop parameters. The short vertical lines at the bottom of the figure indicate the edges of the temperature bins. The $D(T)$ curves are shifted in vertical direction to facilitate comparison.

the product pL only depend on T_i for fixed values of T_a and T_b. Knowledge of the pressure is only of importance when one is interested in the absolute magnitudes of $D(T)$ and L. For the moment we are only interested in the functional shape of the $D(T)$ because that shape determines the relative strengths of lines formed at different temperatures and hence characterizes the spectrum.

As $D(T)$ only depends on the free parameter T_i, it is useful to consider which values T_i can take. From the first integral, the fact that $F_\mathrm{c}(T_\mathrm{a}) = 0$ and the definition of T_i it follows that

$$T_\mathrm{i}^{5/2} = \frac{\frac{2}{7}\left(T_\mathrm{a}^{7/2} - T_\mathrm{b}^{7/2}\right) - F_\mathrm{c,b}^2/(2\kappa_0 E_\mathrm{heat})}{(T_\mathrm{a} - T_\mathrm{b})} \approx \frac{2}{7}T_\mathrm{a}^{5/2} - \frac{F_\mathrm{c,b}^2}{2\kappa_0 T_\mathrm{a} E_\mathrm{heat}} \leq \frac{2}{7}T_\mathrm{a}^{5/2} \quad (9)$$

where we have used that $T_\mathrm{b} \ll T_\mathrm{a}$ in the approximation. From this expression it follows that T_i must be in the range $T_\mathrm{b} \leq T_\mathrm{i} \lesssim 0.6T_\mathrm{a}$. The upper limit for T_i applies to loops with zero conductive flux at the base. Eq. (9) shows that when $F_\mathrm{c,b}^2/E_\mathrm{heat} \ll (4/7)\kappa_0(T_\mathrm{a}^{7/2} - T_\mathrm{b}^{7/2}) \approx (4/7)\kappa_0 T_\mathrm{a}^{7/2}$ the value of T_i, and therefore the shape of $D(T)$, is independent of the conductive flux at the base and the heating. In other words, only a large conductive flux and/or a small heating lead to substantial changes of T_i.

Fig. 2 shows a series of DEMs for constant cross-section loops for the allowed range of T_i. These DEMs were determined from numerical integration of Eqs. (2) and (3). The equations were solved with the boundary conditions $T = T_\mathrm{b}$ and $F = F_\mathrm{c,b}$ at the base and the boundary condition $T = T_\mathrm{a}$ at the apex. Because three boundary conditions for two equations results in an over-determined the system, we assumed an arbitrary value for the heating and used a shooting method combined with the regula falsa to iterate the pressure until the solution satisfied $T = T_\mathrm{a}$ at the apex. Because temperature T_i is determined by the value of E_heat/p^2 an iteration of p with E_heat fixed results in the appropriate values of p and T_i.

The DEMs in Fig. 2 indicate that $D(T)$ is flattest for loops with $F_\mathrm{c,b} = 0$. This is not surprising because for such loops the unbinned $D(T) \rightarrow \infty$ not only at the apex but also at the base, so at T_b. The figure also indicates that for a sufficiently large conductive flux the slope of $D(T)$ becomes independent of the exact value of the conductive flux. In the limiting case $T_\mathrm{i} \rightarrow T_\mathrm{b}$. The results in the figure imply that for a large range of values of T_i the shape of $D(T)$ is insensitive to the exact value of T_i. Thus a DEM analysis can reveal little about the values of E_heat/p^2 and $F_\mathrm{c,b}$. We can rephrase this in the following way: Eq. (5) can be written as

$$F_\mathrm{c,b}^2 = \frac{4\kappa_0}{7}E_\mathrm{heat}\left(T_\mathrm{a}^{7/2} - T_\mathrm{b}^{7/2}\right) - \frac{\kappa_0}{2k^2}p^2\int_{T_\mathrm{b}}^{T_\mathrm{a}} T^{1/2}\Psi(T)dT \ .$$

The apex temperature and the pressure can, in principle, be determined from observations. The expression above shows that the heating E_heat can only be determined when the conductive flux at the base is known. Above we showed that $D(T)$ is largely independent of the conductive flux at the base. When $F_\mathrm{c,b}$ and E_heat cannot be determined also the loop length (Eq. (8)) remains undetermined.

4.2. Loops with increasing cross-sections

The study of loops with increasing cross-sections towards the apex is hampered by the fact that for such loops Eqs. (2) and (3) do not permit to derive a first integral. Numerical simulations show that a variation of the cross-section has only a limited effect on the run of T and F_c in a loop. It was already noted by VAU, that the last term in Eq. (3) can be considered as an extra heating term. Van den Oord & Zuccarello (1997) showed that the effect of this term is a slight lowering of the temperatures T_i and T_a, for given E_heat and p, when compared with a loop with a constant cross-section. But even though loop expansion does not strongly influence the thermodynamical structure of a loop, the varying cross-section strongly modifies $D(T)$ because of the proportionality of $D(T)$ and A (Eq. (4)): a loop with an increasing cross-section towards the apex contains more plasma at higher temperatures and therefore $D(T)$ will be steeper.

Let Γ be the ratio of the cross-sections at the apex and at the base. For geometrically expanding loops ($\Gamma \neq 1$) we assume that these are described by the magnetic field of a buried line dipole (following VAU). In that case the field lines are circles with diameters $2h$ that touch at a depth d below the heights where $T = T_\mathrm{b}$. The expansion factor is given by $\Gamma = h/d$. From (magnetic) flux conservation it follows that the cross-section of a

loop varies as $A(s) = A_\mathrm{b}\Gamma \sin^2(s/h)$ for $h\,\mathrm{arcsin}(1/\sqrt{\Gamma}) \leq s \leq h\pi/2$. Here the cross-section at the base is A_b and s runs from the base (T_b = 3 10^4 K) to the loop apex. Loops with constant cross-sections cannot be described by the field of a line dipole although we usually refer to such loops as $\Gamma = 1$ loops.

The study of expanding loops is facilitated by writing Eqs. (2) and (3) in dimensionless form using the following scaling: $s = s'h$, $T = T'T_\mathrm{a}$, $F_\mathrm{c} = F'\kappa_0 T_\mathrm{a}^{7/2}/h$ and $\Psi(T) = \Psi'(T')\Psi(T_\mathrm{a})$. The dimensionless equations are (dropping the accents)

$$\frac{dT}{ds} = -\frac{F}{T^{5/2}} \quad , \quad \frac{dF}{ds} = \alpha - \beta\frac{\Psi(T)}{T^2} - \frac{2F}{\tan s} \; , \tag{10}$$

with

$$\alpha \equiv \frac{h^2 E_\mathrm{heat}}{\kappa_0 T_\mathrm{a}^{7/2}} \quad \text{and} \quad \beta \equiv \frac{h^2 p^2 \Psi(T_\mathrm{a})}{4k^2\kappa_0 T_\mathrm{a}^{11/2}} \; . \tag{11}$$

The following boundary conditions apply

base: $s = \mathrm{arcsin}(1/\sqrt{\Gamma})$, $T = T_\mathrm{b}/T_\mathrm{a}$, $F = \frac{F_\mathrm{c,b}h}{\kappa_0 T_\mathrm{a}^{7/2}} \equiv F'_\mathrm{b}$
apex: $s = \pi/2$, $T = 1$, $F = 0$

Because we have four boundary conditions and only two equations we iterated the solution (Newton iteration), using α and β as free parameters, until the solution satisfied the boundary conditions. It turns out that when the dimensionless conductive flux at the base $F'_\mathrm{b} \equiv hF_\mathrm{c,b}/(\kappa_0 T_\mathrm{a}^{7/2})$ is varied in a continuous way, with T_b, T_a and Γ fixed, also α and β behave continuously. When for a value of F'_b, α and β have been determined, one can integrate the system of differential equations and determine $D(T)$. The relation between α, β and F'_b is shown in Fig. 3a for T_a = 4 MK, Γ = 5 and Γ = 50. The figure shows that when $|F'_\mathrm{b}|$ increases, both α and β decrease. Note that $F'_\mathrm{b} \leq 0$ because $F_\mathrm{c,b} \leq 0$. There exists a maximum for $|F'_\mathrm{b}|$ at which β becomes zero. At this maximum, heating balances conduction without radiative losses. For larger values of $|F'_\mathrm{b}|$ physically meaningful solutions do not exist. In Fig. 3b we show $D(T)$ as a function of F'_b for Γ = 5 and Γ = 50. For each value of Γ the upper curve corresponds to the DEM of a loop with zero conductive flux at the base while the lower curve is the DEM for a loop with $\beta = 0$. The steepness of $D(T)$ increases with increasing $|F'_\mathrm{b}|$, but, on the other hand, the typical shape of $D(T)$ does not show strong variations. In Fig. 3b we only show the cases Γ = 5 and Γ = 50. Γ and F'_b can, however, take any value which makes it impossible to determine these quantities from the shape of $D(T)$. In other words, loops with different values of Γ and F'_b, can have (almost) identical DEMs and therefore emit (almost) identical spectra. The model DEMs shown in Fig. 3b are strongly peaked towards the apex temperature and, as a consequence, the corresponding spectra contain mainly lines formed at, or close to, the apex temperature. Because of the finite temperature range over which lines contribute it is difficult, if not impossible, to distinguish between a large expansion factor Γ and a large value of $|F'_\mathrm{b}|$.

Suppose now that we know the values of Γ and F'_b, despite the fact that we showed above that these cannot be determined

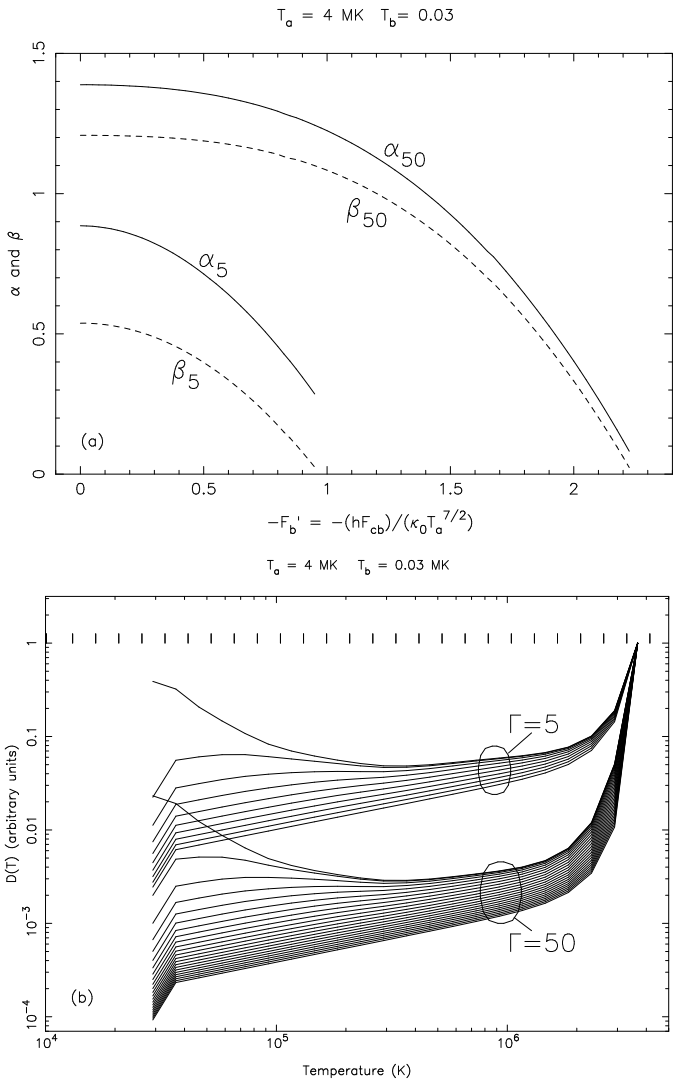

Fig. 3. a Dimensionless coronal loop parameters α (solid) and β (dashed) – Eq. (11) – as a function of the dimensionless conductive flux at the base F'_b. The apex temperature is fixed at 4 MK. The upper two curves are for an expansion factor Γ = 50 and the lower-left curves for Γ = 5. When β reaches zero, physical solutions cease to exist. **b** Model DEMs for different values of F'_b. The upper set of curves is for Γ = 5 and the lower set for Γ = 50. In each set the upper curve is for F'_b = 0 and the lower curve for the maximum value of $|F'_\mathrm{b}|$ for which β = 0. Between successive curves F'_b is decreased with 0.1.

from observed spectra. When $|F'_\mathrm{b}|$, and therefore α and β are known, one also knows the values of $hF_\mathrm{c,b}$, h^2E_heat and hp. A determination of one of these parameters fixes the others. Observationally one can only determine the pressure using density-sensitive lines. When this diagnostic tool is available one can also determine h, E_heat and $F_\mathrm{c,b}$.

Above we showed that there is a maximum value for $|F'_\mathrm{b}|$. For practical purposes it is useful to know how large $|F'_\mathrm{b}|$ can be. In the limiting case, radiative losses are not important and can be neglected. The equations permit then an analytical solution

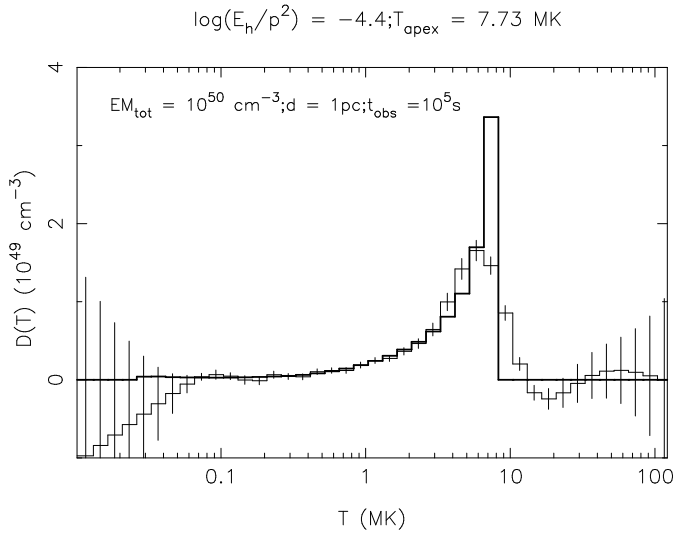

Fig. 4. Model DEM of a quasi-static coronal loop (thick solid) and the DEM recovered by means of statistical regularization (line with error bars).

which can be used to determine the minimum values of α and $F_{\rm b}'$:

$$\alpha > \frac{4}{7}\left(1-\left(\frac{T_{\rm b}}{T_{\rm a}}\right)^{7/2}\right)\left(\cot(\arcsin\frac{1}{\sqrt{\Gamma}})\arccos\frac{1}{\sqrt{\Gamma}}\right)^{-1},$$

$$F_{\rm b}' > -\frac{2}{7}\left(1-\left(\frac{T_{\rm b}}{T_{\rm a}}\right)^{7/2}\right)\Gamma\frac{\arccos\frac{1}{\sqrt{\Gamma}}+\frac{1}{\sqrt{\Gamma}}\cos(\arcsin\frac{1}{\sqrt{\Gamma}})}{\cot(\arcsin\frac{1}{\sqrt{\Gamma}})\arccos\frac{1}{\sqrt{\Gamma}}}.$$

In these expressions $T_{\rm a}$ and $T_{\rm b}$ are the dimensional temperatures. These analytic expressions for the limiting values of α and $|F_{\rm b}'|$ correspond very well with the numerical results.

5. Application of loop models to *EUVE* DEMs

5.1. Global comparison of stellar and model DEMs

In this section we compare the observed DEMs with realizations of theoretical DEMs as these would be reconstructed from *EUVE* observations. For illustrative purposes we show in Fig. 4 a theoretical input DEM for a loop with constant cross-section and zero conductive flux at the base. This DEM has a pronounced maximum in the bin that contains $T_{\rm a}$ reflecting that a coronal loop is to a large extent isothermal. The recovered DEM follows the model DEM reasonably well but extends two temperature bins beyond the theoretical DEM. This is to be expected both because spectral lines have a natural formation width of $\Delta\log T \approx 0.3$, or three temperature bins, and because the regularization smooths over an interval that matches this formation width. Fig. 4 is characteristic of other comparisons of model and recovered DEMs with apex temperatures between 0.5 MK and ∼20 MK. For higher temperatures the lack of spectral lines in the *EUVE* bandpass leads to a poor recovery. The left-hand tail in the theoretical input DEM weights $D(T)$ away from $T_{\rm a}$ towards a slightly lower temperature. When $\Gamma > 1$ the theoretical input DEM is so strongly peaked at $T_{\rm a}$ that also the recovered DEM has its maximum very close to $T_{\rm a}$.

In order to compare empirical stellar DEMs with recovered model DEMs we proceeded as follows. Coronal loop models, and the related DEMs, were calculated following the method outlined in Sect. 4. The model DEMs were scaled to a total emission measure of 10^{50} cm^{-3}. Spectra were generated for those DEMs, including photon noise, assuming an observing time of 10^5 s, a distance of 1 pc and a hydrogen column density of 10^{18} cm^{-2}. The DEMs were scaled so that their maxima correspond to unity. For each stellar system the loop apex temperature was taken equal to the temperature at which the empirical DEM has its maximum. Models were then calculated for expansion factors Γ =1, 2, 3, 5 and 10. For each of these expansion factors the cases $F_{\rm c,b} = 0$ and $F_{\rm c,b} \neq 0$ were considered. When $F_{\rm c,b} \neq 0$ the parameters $T_{\rm i}$ (for $\Gamma = 1$) and $F_{\rm b}'$ (for $\Gamma \neq 1$) were chosen to correspond approximately to the steepest possible DEM at that value of Γ. We thus compare the extremes of all possible DEMs at a given Γ.

Because in Papers I and II we found evidence for abundance deviations, we made for each model DEM model spectra with solar photospheric abundances and with the Fe abundance half of its solar photospheric value. DEM analyses were then performed under the assumption of solar abundances to study the effect of errors in the assumed abundances

In Figs. 5-8 we compare the observed and simulated DEMs for Capella, χ^1 Ori, ξ UMa and α Cen. Each figure has the following general layout:

	$F_{\rm b}=0$ Fe = 1	$F_{\rm b}=0$ Fe = 0.5	$F_{\rm b}\neq 0$ Fe = 1	$F_{\rm b}\neq 0$ Fe = 0.5
$\Gamma = 1$	a	b	c	d
$\Gamma = 2$	e	f	g	h
$\Gamma = 3$	i	j	k	l
$\Gamma = 5$	m	n	o	p
$\Gamma = 10$	q	r	s	t

For some sources we show a restricted set of panels (see captions). The error bars of the recovered model DEMs are comparable to the error bars of the stellar DEMs. The figures do not represent best-fit results, but indicate specific trends when $T_{\rm a}$ is kept fixed.

Figs. 5-8 indicate that an increase of the expansion factor Γ makes the DEM increasingly narrow, although for large Γ the sensitivity decreases. The DEMs with zero conductive flux at the base and those for a large conductive flux at the base do not differ significantly within the temperature range shown.

The simulations with a reduced Fe abundance (columns two and four) result in small 'fluctuations' in the DEM at temperatures in the range 0.1 MK–2 MK. This can be understood by the fact that most emission lines in *EUVE* spectra are from iron. If the iron abundance is reduced in the model spectra, lines of other elements become relatively more important and start to influence the DEM. In the temperature range shown, an erroneous assumption about the abundances in the source seems to have little effect on the recovered DEM, however.

The figures confirm that it is often impossible to discriminate between loops with a large expansion factor and zero conductive flux at the base and loops with a smaller expansion factor having a large conductive flux at the base. Compare, for example, in Fig. 6 k and m, l and n.

For Capella, χ^1 Ori and ξ UMa Figs. 5, 6 and 7 (top rows) show that the observed DEMs are incompatible with loops with constant cross-sections, even when a large conductive flux is invoked. For these objects the observed DEMs indicate that, when the presence of a single loop population is assumed, Γ must be roughly in the range 3–5. For α Cen (Fig. 8) the DEM is not compatible with an interpretation in terms of a single loop population: the left-hand flank of the DEM of α Cen shows a small bump that can be reproduced when a second loop population with a slightly lower temperature is introduced.

It is of course likely that loops with different apex temperatures are present in stellar coronae, like on the Sun. Moreover, there can be contributions from loops near the limb which are partly obscured by the star. For χ^1 Ori, it seems that the observed DEM can nevertheless be mimicked by a single population of coronal loops. Fig. 6 shows that the observed DEM extends over 3 bins on both sides of the maximum. This is what would be expected of an almost isothermal plasma. Both strong expansion and a strongly non-zero conductive flux make a DEM almost isothermal. For χ^1 Ori we conclude that the observed DEM can be explained with a single loop population with $\Gamma \gtrsim 3$.

The recovered DEM of a single coronal loop is characterized by a drop of $D(T)$ within three temperature bins above $T_{\rm a}$. The observed DEM for α Cen (Fig. 8) shows this property. The right-hand flanks of the stellar DEMs of Capella and ξ UMa drop over five temperature bins, which is slower than would be expected from a single loop population. For these objects the observed DEM can be reproduced better when a second loop population at slightly higher temperatures is included.

In Fig. 9 we show the stellar and recovered model DEMs for α Cen, Capella and ξ UMa for the case that two coronal loop populations contribute to the observed emission. The parameters of the loop components are given in the figures. For each loop component we give Γ, $T_{\rm a}$ and $F'_{\rm b}$. In principle we could also give the values of α and β which, in combination with density (diagnostics), would allow the calculation of the lengths of the loops, the heating, the conductive flux at the base etc.. We stress, however, that the parameters of the loop components are rather arbitrary when $\Gamma \gtrsim 3$. In principle we could replace each of these components by one with a larger/smaller expansion factor and a smaller/larger conductive flux at the base. This shows the arbitrariness of fitting coronal loop models to observed DEMs: different models, with essentially identical simulated DEMs, can result in a range of values for $F'_{\rm c,b}$ (and α and β) so that some fundamental parameters of the loops cannot be determined unambiguously.

Paper II gives an electron density for Capella in the range $10^{12} - 2\ 10^{13}$ cm^{-3} as derived from density-sensitive line ratios for lines formed at temperatures 6 – 11 MK. The coronal loop component at 8.2 MK is within this temperature range. For T = 8.2 MK the scaling law (Rosner et al. 1978) results in a loop half length of $L \approx 84/n_{13}$ km ($n_{13} = n/10^{13}$ cm^{-3}). Although this value is very small, it does not necessarily conflict with a coronal loop interpretation. Therefore we consider the confinement and the heating requirements. The gas pressure equals $p = 2\ 10^4\ n_{13}$ dyne cm^{-2}. Confinement requires a magnetic field of at least $B_{\rm min} = 700\ \sqrt{n_{13}}$ G which is feasible for low-lying, short loops. The heating must exceed the radiative losses, so that $E_{\rm heat} \gtrsim E_{\rm rad} \approx n^2\Psi_0/\sqrt{T} = 5\ 10^3\ n_{13}^2$ erg cm^{-3}s^{-1}. Suppose that the heating is related to dissipation of magnetic field, then the typical dissipation time scale is $\tau_{\rm diss} = B^2/(8\pi E_{\rm heat}) \lesssim 9B_3^2/n_{13}^2$ sec., with B_3 in units of 10^3 G. This expression shows that the magnetic field is dissipated on a time scale of seconds. For a density of 10^{12} cm^{-3} this time scale increases to only fifteen minutes. This implies that the corresponding coronal structures are ephemeral compared to the exposure time, with many different features lighting up only briefly. As an alternative we can argue that the heating is related to wave dissipation. The required energy flux in the waves can be estimated from $F_{\rm wave} = E_{\rm heat} L \gtrsim 5\ 10^{10}\ n_{13}$ erg cm^{-2}s^{-1}. This value is close to the bolometric flux density of the star, so that, even if it could be produced locally for brief periods of time, the conclusion must again be that the emitting features are ephemeral. The same problems arise for the 10 – 20 MK plasma on ξ UMa with $n \sim 5\ 10^{12}$ cm^{-3} (paper II). The high densities found can be explained if one considers what happens in a volume subjected to intense heating. The temperature increases dramatically while the radiative losses drop. As a consequence there will be a large conductive flux leading to chromospheric evaporation so that the density will increase until a balance is reached. For a density of 10^{12} cm^{-3} the radiative loss time is one minute which is shorter than the dissipative time scale of fifteen minutes. In that case the heating time scale exceeds the time scale for the losses so that *temporarily* a quasi-static loop can exist and the scaling law applies. For densities of the order of 10^{13} cm^{-3} both the dissipative and the radiative time scales are of the order of seconds, which is not reconcilable with the notion of a quasi-static equilibrium.

6. Discussion and conclusions

In this paper we discuss spectroscopic inversions to obtain information about physical conditions prevailing in coronae of cool stars. This process is limited by three intrinsic problems. First, there is the problem that quasi-static loops with very different parameters emit identical spectra: if the products $hF_{\rm c,b}$, $h^2E_{\rm heat}$ and hp are kept constant, together with the apex temperature, only density-sensitive lines will differ from spectrum to spectrum. Second, the thermal structure as characterized by the differential emission measure (DEM) for loops with the same apex temperature, but different combinations of dimensionless base conductive flux $F'_{\rm b}$ and expansion factor Γ, can be very nearly the same, signaling that the spectra will be nearly the same, particularly in view of the following problem. Inversion of the Fredholm equation (Eq. (1)), that relates the DEM and the observed spectrum, a) is limited by the substantial width of the temperature interval over which individual lines form, b)

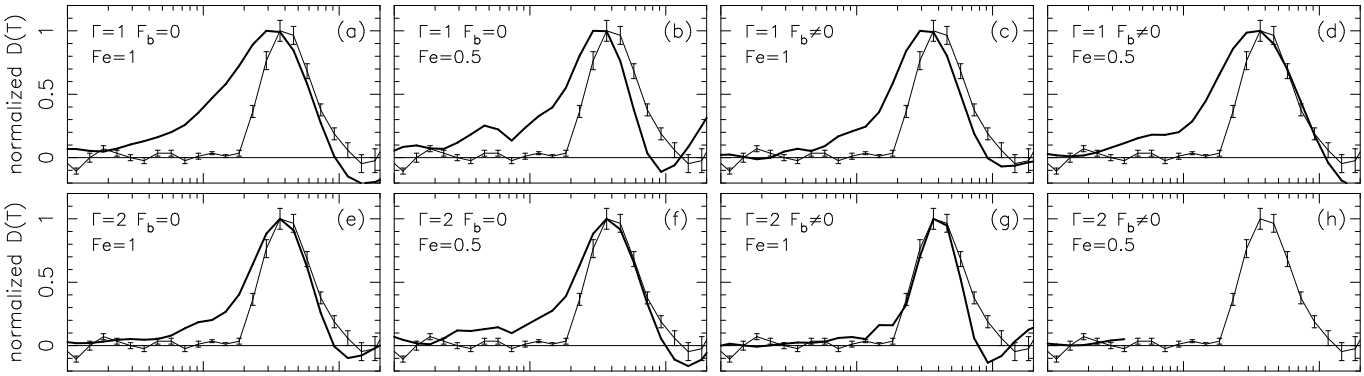
normalized D(T)
Γ=1 F_b=0
Fe=1
(a)
Γ=1 F_b=0
Fe=0.5
(b)
Γ=1 F_b≠0
Fe=1
(c)
Γ=1 F_b≠0
Fe=0.5
(d)
normalized D(T)
Γ=2 F_b=0
Fe=1
(e)
Γ=2 F_b=0
Fe=0.5
(f)
Γ=2 F_b≠0
Fe=1
(g)
Γ=2 F_b≠0
Fe=0.5
(h)
0
0.5
1

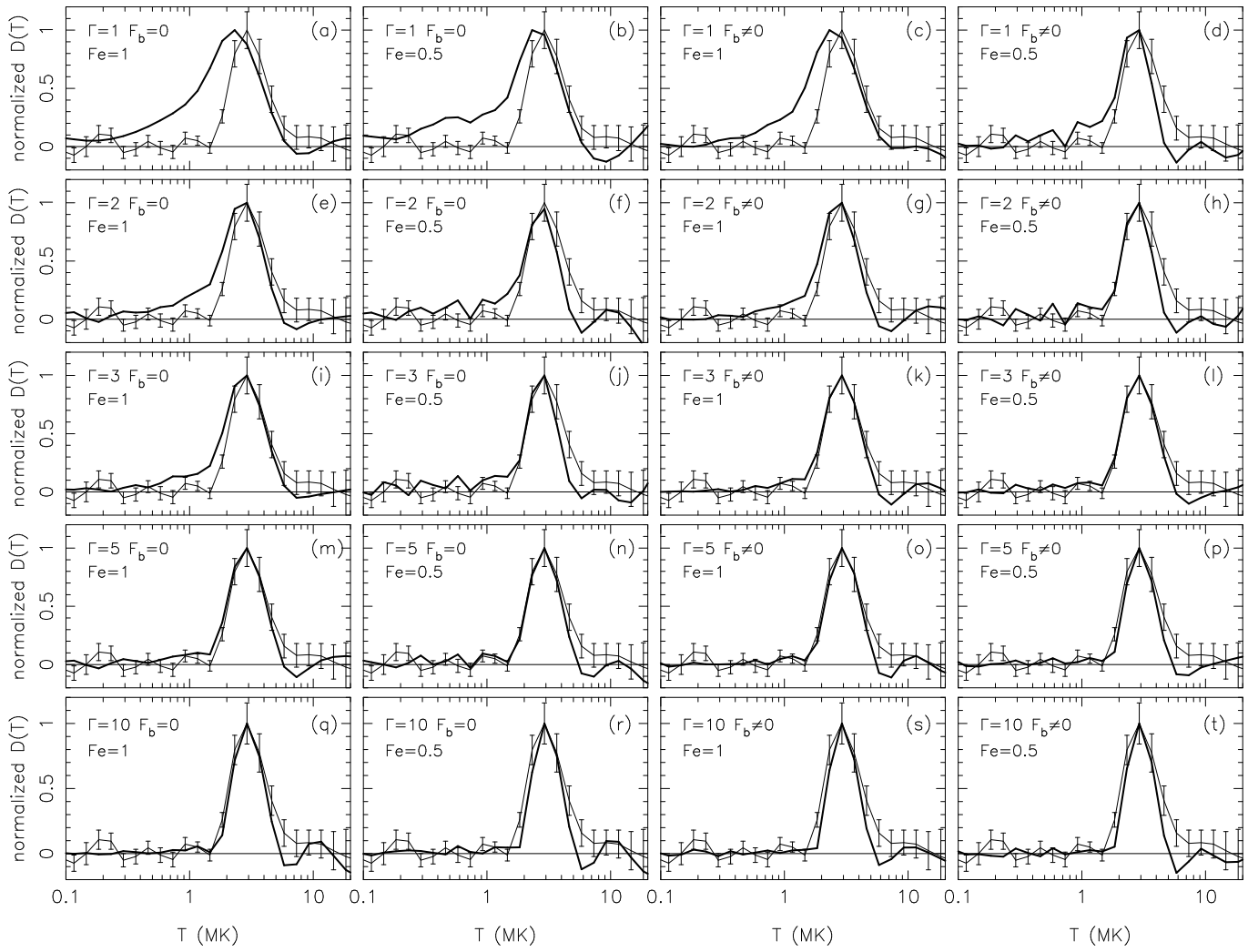

Fig. 6a–t. χ^1 Ori: observed DEM (thin line with error bars) and simulated model DEM (thick line). In the simulations the apex temperature is fixed at 3.11 MK. The rows from top to bottom are for expansion factors Γ = 1, 2, 3, 5 and 10 respectively.

erated by varying $F'_{\rm b}$. The uncertainty in Γ is, therefore, related to an uncertainty in $F'_{\rm b}$ and, as a consequence, to an uncertainty in α and β. The parameters $F'_{\rm b}$, α and β can, in combination with a measured density, be used to derive the loop length, the heating and the conductive losses through the base. Even if one is able to determine the density with infinite accuracy, there is still an intrinsic uncertainty in the derived parameters because of the uncertainty in the determination of Γ.

In this paper we only considered loops with constant pressure. This is correct as long as the height of a loop is smaller than the coronal scale height. The effect of hydrostatic equilibrium on the thermodynamical structure of a loop is small: only the temperature $T_{\rm i}$ is slightly lowered (see van den Oord & Zuccarello, 1996, 1997). Hydrostatic equilibrium affects the DEM, however, because of the $D(T) \propto p$ dependence, and makes the DEM slightly flatter. For loops, whose heights exceed the scale height, the quantitative effect of hydrostatic equilibrium is difficult to estimate because one needs to know the component of the gravitational acceleration along the field which depends on the (unknown) field line topology. Therefore we restricted ourselves to loops with constant pressure.

For α Cen, Capella, ξ UMa and χ^1 Ori we have investigated whether the observed DEMs are compatible with a coronal loop interpretation. For all stellar systems, but α Cen, we found that the observed DEM distributions are incompatible with those of coronal loops with constant cross-section, regardless of the conductive flux at the base; the cool flank of the observed DEMs is simply too steep. For α Cen we cannot rule out an interpretation in terms of constant cross-section loops with a substantial base conductive flux (Fig. 8c), but the agreement is not convincing in the temperature range $0.2 - 0.9$ MK. A more acceptable fit is found for α Cen when a second population of loops is introduced with $T_{\rm a}$ = 1.2 MK. Because the difference between the observed and the simulated DEM is never more than 2σ, we consider the remaining differences to be statistically insignificant.

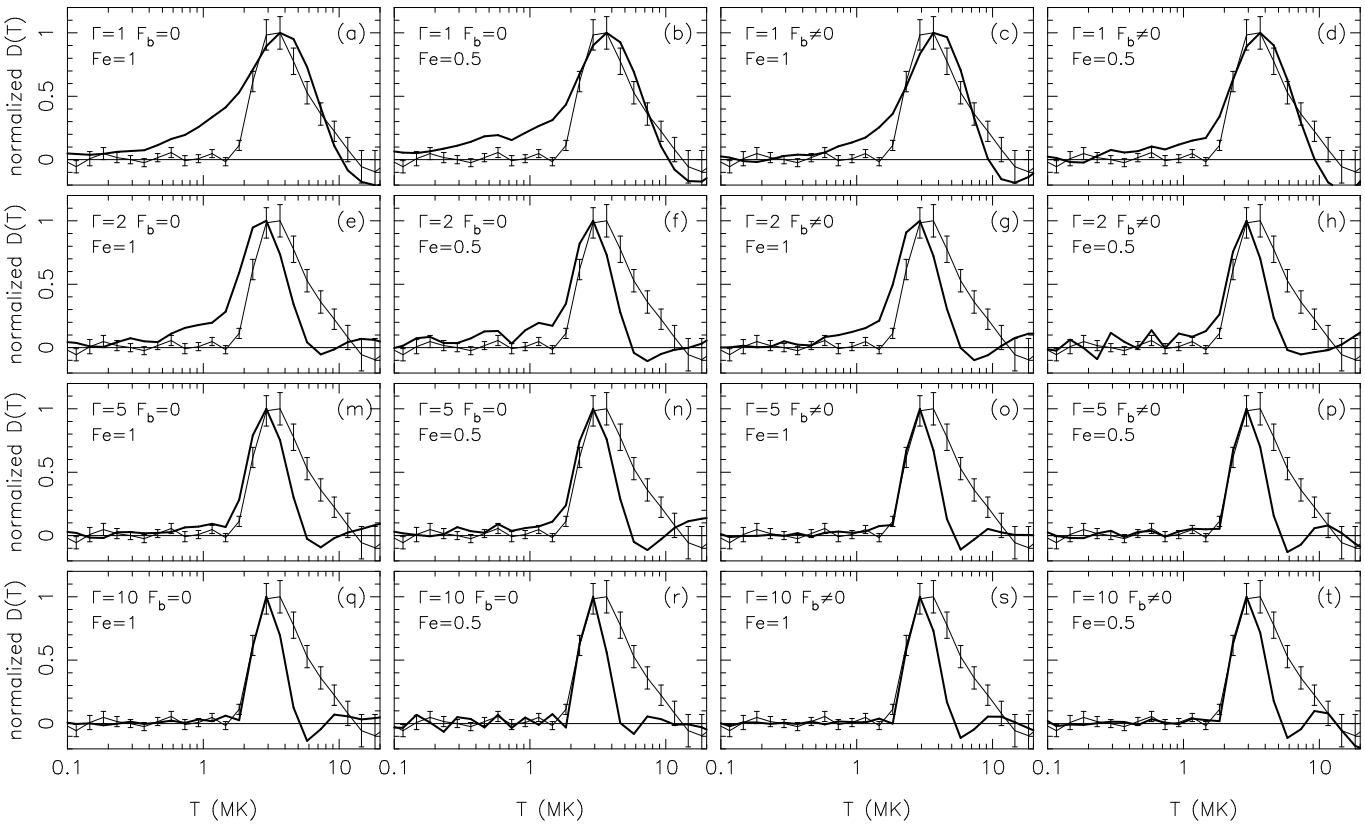

Fig. 7a–t. ξ UMa: observed DEM (thin line with error bars) and simulated model DEM (thick line). In the simulations the apex temperature is fixed at 4.93 MK. The rows from top to bottom are for expansion factors Γ = 1, 2, 5 and 10 respectively.

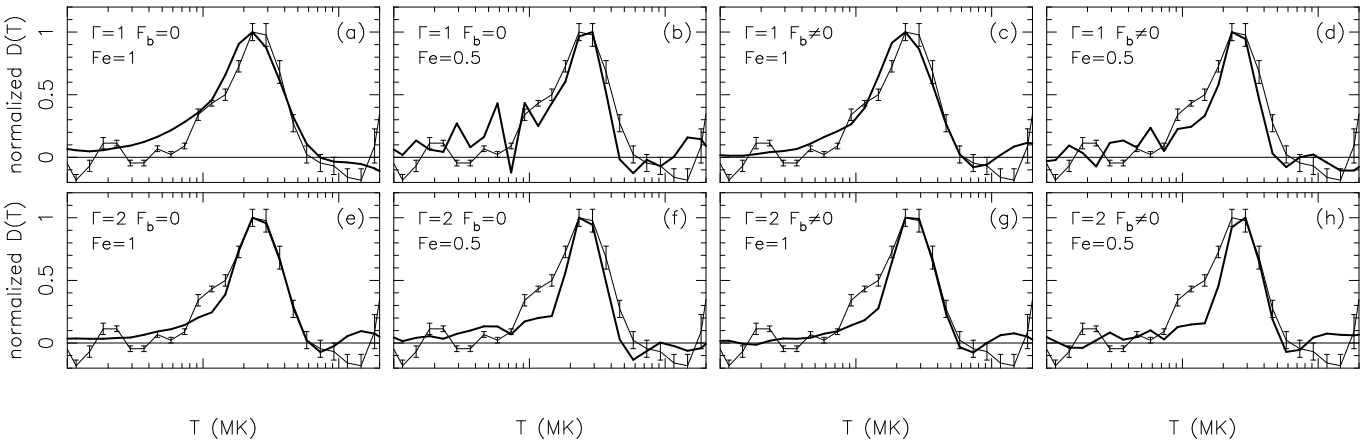

Fig. 8a–h. α Cen: observed DEM (thin line with error bars) and simulated model DEM (thick line). In the simulations the apex temperature is fixed at 2.83 MK. The top row is for expansion factor Γ = 1 and the bottom row for expansion factor Γ = 2.

The DEM of χ^1 Ori can be satisfactorily explained by expanding loops with $\Gamma \approx 3-5$ or larger. The observed DEM of χ^1 Ori is very narrow with both flanks extending over a factor two in temperature, indicating only a small spread in the intrinsic coronal temperatures. For Capella and ξ UMa we need to invoke at least two loop populations, both with moderate expansion and possibly with a non-negligible conductive flux at their base.

We investigated whether the DEM of χ^1 Ori can be explained by an ensemble of loops with large expansion factors ($\Gamma \approx 50$) and a small spread of apex temperatures instead of one loop population with a moderate expansion factor and a single apex temperature. This did not result in acceptable re-

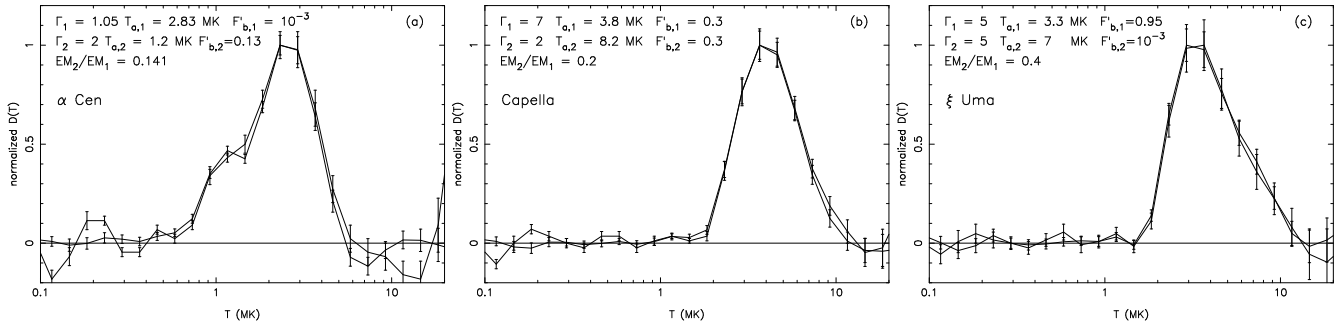

Fig. 9a–c. Stellar (thin solid lines) and simulated model (thick solid lines) DEMs for **a** α Cen, **b** Capella and **c** ξ UMa. The model DEMs comprise two distinct components whose total emission measures are indicated by EM_1 and EM_2. For each of these components the apex temperature T_a, the expansion factor Γ and the dimensionless conductive flux F_b' are given. Note that the values of Γ and F_b' are not uniquely determined.

covered DEMs for the following reason. For expanding loops the high temperature part of the DEM varies approximately like $D(T) \propto \exp[\mu(T-T_\mathrm{a})]$ with μ a constant depending on Γ. This shape is very specific and cannot be mimicked by summing the DEMs of loops with larger expansion factors, corresponding to relatively larger values of μ, and slightly different apex temperatures. In other words, the DEMs of strongly expanding loops are almost isothermal but not to the extent that an arbitrary DEM can be decomposed into their contributions.

Our result that for all considered sources (except possibly α Cen) coronal loops *must* be geometrically expanding is consistent with the results by Schrijver et al. (1989) for Capella and σ^2 CrB with the *EXOSAT-TGS*. The expansion factors we quote in this paper and those found by Schrijver et al. are difficult to compare. Schrijver et al. only considered expanding loops with zero conductive flux at the base. As we discussed in this paper, the inclusion of a finite base flux can lower the required expansion factor. Therefore also the values of Γ and F_b' shown in Fig. 9 are subject to intrinsic uncertainties.

The high plasma densities found for Capella and ξ UMa cannot be related to a long-lived coronal loop population because of the energy requirements. The high densities imply small volumes of intense coronal heating. We hypothesize that the high densities are related to a large number of compact (< 1000 km) structures, with a small surface filling factor, which brighten briefly.

Our results indicate that care has to be exercised when decomposing an observed spectrum into the spectral contributions by one or more coronal loops. The parameters of the 'best-fit' model do not necessarily describe the loops in the observed corona. Only the parameter combinations $hF_\mathrm{c,b}$, h^2E_heat and hp can be determined with limited accuracy because of the uncertainty in the value of the expansion factor. It is, however, possible to interpret the stellar DEMs of α Cen, Capella, χ^1 Ori and ξ UMa in terms of quasi-static loop models. Contrary to static models, quasi-static models do allow for the presence of dynamical phenomena like, e.g., plasma flows, but to the extent that the global energy balance is still dominated by a balance between heating, conduction and radiation. For the $EUVE$ observations we found that it is not necessary to invoke other types of coronal loop models.

Acknowledgements. We thank the referee Dr. M. Güdel for constructive criticism. GHJvdO acknowledges financial support from the Netherlands Organization for Scientific Research (NWO). SRON is financially supported by NWO.

References

Anders E., Grevesse N., 1989, Geochimica et Cosmochimica Acta 53, 197
Arnaud M., Rothenflug R., 1985, A&AS 60, 425
Arnaud M., Raymond J., 1992, ApJ 398, 394
Bowyer S., Malina R.F., 1991, Extreme Ultraviolet Astronomy, eds. R.F. Malina, S. Bowyer, Pergamon Press, New York, p. 397
Bowyer S., Malina R.F., 1996, IAU Coll. 152: Astrophysics in the Extreme Ultraviolet, Kluwer, Dordrecht
Craig I.J.D., Brown J.C., 1976, A&A 49, 239
Craig I.J.D., Brown J.C., 1986, Inverse problems in astronomy, Bristol: Adam Hilger Ltd, Bristol, England.
Ciaravella A., Peres G., Maggio A., Serio S., 1996, A&A 306, 553
Ciaravella A., Magio A., Peres G., 1997, A&A 320, 945
Harrison R.A, Thompson A.M. (eds.), 1991, Intensity Integral Inversion Techniques: a Study in Preparation for the SOHO mission, Rutherford Appleton Lab. Report RAL-91-092
Hubeny V., Judge P.G., 1995, ApJ 448, L61
Judge P.G., Hubeny V., Brown J.C., 1997, ApJ 475, 275
Kaastra J.S., Mewe R., Liedahl D.A., et al., 1996a, A&A 314, 547
Kaastra J.S., Mewe R., Nieuwenhuijzen H., 1996b, in UV and X-ray spectroscopy of astrophysical and laboratory plasmas, eds. K. Yamashita, T. Watanabe, Univ. Acad. Press, p. 411
Maggio A., Peres G., 1996, A&A 306, 563
Mewe R., Kaastra J.S., Schrijver C.J., van den Oord G.H.J., Alkemade F., 1995, A&A 296, 477 (Paper I)
Mewe R., Kaastra J.S., White S.M., Pallavicini R., 1996a, A&A 315, 170
Mewe R., van den Oord G.H.J., Schrijver C.J., Kaastra J.S., 1996b, in IAU Symp. 152: Astrophysics in the Extreme Ultraviolet, eds. S. Bowyer, R.F. Malina, Kluwer, p.553
Press W.H., Flannery B.P., Teukolsky S.A., Vetterling W.T., 1992, Numerical Recipes, Cambridge: Cambridge University Press
Rosner R., Tucker W.H., Vaiana G.S., 1978, ApJ 220, 643

Schmitt J.H.M.M., Drake J.J., Haisch B.M., Stern R.A., 1996, ApJ 467, 841
Schrijver C.J., Lemen J.R., Mewe R., 1989, ApJ 341, 484
Schrijver C.J., van den Oord G.H.J., Mewe R., 1994, A&A 289, L23
Schrijver C.J., Mewe R., van den Oord G.H.J., Kaastra J.S., 1995, A&A 302, 438 (Paper II)
Schrijver C.J., van den Oord G.H.J., Mewe R., Kaastra J.S., 1996, in IAU Symp. 152: Astrophysics in the Extreme Ultraviolet, eds. S. Bowyer, R.F. Malina, Kluwer, p.121
Spitzer L., 1962, Physics of fully ionized gasses, Interscience, New York
van den Oord G.H.J., Barstow M.A., 1988, A&A 207, 89
van den Oord G.H.J., Zuccarello F., 1996, in IAU Symp. 176: Stellar Surface Structure, eds. K.G. Strassmeier, J.L. Linsky, Kluwer, p. 433
van den Oord G.H.J., Zuccarello F., 1997, A&A, submitted
Vesecky J.F., Antiochos S.K., Underwood J.H., 1979, ApJ 233, 987 (VAU)

This article was processed by the author using Springer-Verlag LaTeX A&A style file *L-AA* version 3.